Hindawi
Journal of Nanomaterials
Volume 2022, Article ID 5531041, 16 pages
https://doi.org/10.1155/2022/5531041

Research Article

Prescribed Thermal Activity in the Radiative Bidirectional Flow of Magnetized Hybrid Nanofluid: Keller-Box Approach

Iftikhar Ahmad,[1] Qazi Zan-Ul-Abadin,[1] Muhammad Faisal,[1] K. Loganathan,[2,3] Tariq Javed,[4] and Dinesh Kumar Chaudhary[5]

[1]*Department of Mathematics, Azad Jammu & Kashmir University, Muzaffarabad 13100, Pakistan*
[2]*Research and Development Wing, Live4Research, Tiruppur, Tamilnadu 638106, India*
[3]*Department of Mathematics and Statistics, Manipal University Jaipur, Jaipur, 303007 Rajasthan, India*
[4]*Department of Mathematics and Statistics, International Islamic University, Islamabad 44000, Pakistan*
[5]*Department of Physics, Amrit Campus, Tribhuvan University, Kathmandu, Nepal*

Correspondence should be addressed to Qazi Zan-Ul-Abadin; qazi.zain@ajku.edu.pk, K. Loganathan; loganathankaruppusamy304@gmail.com, and Dinesh Kumar Chaudhary; din.2033@gmail.com

Received 5 May 2022; Revised 9 June 2022; Accepted 16 July 2022; Published 27 July 2022

Academic Editor: Zafar Said

In this exploration, we decided to investigate the significance of prescribed thermal conditions on unsteady 3D dynamics of water-based radiative hybrid nanofluid with the impact of cylindrical-shaped nanosized particles (alumina (Al_2O_3) and titania (TiO_2)). For physical relevancy, the impact of the Lorentz force is also included. The combination of suitable variables has been used to transform the transport equations into the system of ordinary differential equations and then numerically solved via the Keller-Box approach. Graphical illustrations have been used to predict the impact of the involved parameters on the thermal setup. Convergence analysis is presented via the grid independence approach. Skin frictions and local Nusselt numbers against various choices of involved parameters are plotted and arranged in tabular forms. It is observed through the present investigation that temperature distribution is increased with the higher choices of radiation parameter $0.0 \le R_d \le 2.0$ and decreased with the improvement in the choices of temperature maintaining indices (i.e., $-2.0 \le r, s \le 2.0$). Moreover, the thermophysical properties except specific heat for hybrid nanofluid are improved with the involvement of cylindrical-shaped nanoparticles. The temperature of the hybrid nanofluid is observed to be higher for variable thermal conditions as compared to uniform thermal conditions. Outfalls for a limited version of the report have been compared with a previous published paper.

1. Introduction

Nanofluids have been widely used in many technological and industrial processes like nuclear reactors, automobile radiators, and solar aircrafts because their superior thermal conductivity as compared to conventional fluids as the rate of heating/cooling is extremely reliant on the performance of thermal conductivity of the nanosized particles. Various mathematical relations [1, 2] have been adopted to investigate the thermophysical properties of nanosized particles but the most appropriate mathematical relations regarding these properties are developed/discussed by Masoumi et al. [3]. The boundary regime flow of nanofluid due to an expanding device is firstly numerically deliberated by Khan and Pop [4] with random motion and thermodiffusion effects of tiny-sized particles. Sheikholeslami and Rokni et al. [5] elaborated the heat transfer mechanism by using single-phase and double-phase estimations of magneto-nanofluid and proved that higher estimation of tiny particle concentration augments the temperature gradient. Ganvir et al. [6] summarized the combined performance of convective heat transference, particle size, thermophysical properties, inlet velocity, volume concentration, and liquid temperature, both analytically and numerically.

An improved approach to overcome the thermal needs of industrial and engineering processes is famous with the name of hybrid nanofluid. The investigation about the

importance of hybrid nanofluid has gained a tremendous height due to their wide applications in domestic refrigerators, engine cooling, microelectronics, heat exchanger devices, pharmaceutical processes, fuel cells, grinding processes, ultrasonic radiations, thermal diffusion processes, and many more. Hybrid nanofluid can be formed by submerging two or more nanoparticles into the host liquid. These nanoparticles may include metals, dielectrics, liquid materials, polymeric, lipids, and semiconductors. Some common examples of nanoparticles are copper, zinc-oxide, carbon nanotubes, phosphates, zinc sulfide, cadmium telluride, etc. Alumina and titania nanoparticles are widely used in engineering applications, and these are prepared from metal precursors. These tiny-sized particles can be synthesized by electrochemical, chemical, or photochemical methods. These nanoparticles have commercial applications due their structure, high strength, electron affinity, and electrical conductivity. The most widely used oxide ceramic material is alumina, and it has applications in cutting tools, tap washers, spark plugs, etc. The most abundantly used nanomaterial for human life is titania, and it is used in sunscreen, biomedical applications, photovoltaic devices, pharmaceutical drugs, and waste water treatment and as a food additive. Sarkar et al. [7] reviewed the advantages and disadvantages of nano as well as hybrid nanofluids and recommended that hybrid nanofluids have various advantages as compared to conventional nanofluids because of their auspicious heat transference enhancement, pressure drop ability, improved thermal network, and favorable aspect ratio. Sidik et al. [8] disclosed the recent progress related to the field of hybrid nanofluids by discussing the factors affecting their thermal properties and stability. Unsteady dynamics of hybrid nanofluid with heat transference characteristic due to the expanding/contracting device is numerically explored by Waini et al. [9] and presented the stability analysis regarding the dual solutions. Numerical evaluation regarding pure water-based hybrid nanofluids with the combination of nanoparticles (alumina, titania, and silica) is explored by Minea [10]. Investigation concerning water-based hybrid nanofluids with the optical properties of titania and alumina nanoparticles is made by Leong et al. [11] along the stability of the obtained solution. Moldoveanu et al. [12] glimpsed the experimental evaluation regarding the hybrid mixture of alumina and titania nanoparticles with viscosity as the main focus of the investigation. Moldoveanu et al. [13] also evaluated the hybrid mixture of titania and alumina nanoparticles with thermal conductivity as the foremost point of the exploration. Shirazi et al. [14] experimentally discussed the mixture of titania nanoparticles and water in order to observe the level of the oil recovery enhancement process. Khan et al. [15] elaborated the mixed convective stagnation dynamics of the radioactive mixture of titania, copper, and water in the magnetic environment towards an expandable device. An experimental evaluation regarding the stability, characterization, and dynamic viscosity of the hybrid mixture of titania and cupric oxide with water as working fluid is completed by Asadi et al. [16]. Ahmad et al. [17] explained the heat/mass transference attributes in the hybrid interpretation of alumina and copper nanoparticles through porous media. A comparative depiction regarding unsteady transport of magnetically influenced water-based fluid with the hybrid mixture of nanoparticle combinations (copper-alumina and alumina-titania) towards an expanding device using finite element approach is elaborated by Ali et al. [18]. Some recent scientific contributions about hybrid nanofluids have been addressed by some scholars/researchers (refs. [19–21]) and their applications (refs. [22–26]).

In the last few years, researchers are interested to discuss the novel impact of the shape of nanoparticles in the improvement of heating/cooling processes, solar aircrafts, effective thermal conductivity, and other thermophysical characteristics. Zhang et al. [27] measured the values of effective thermal conductivity and thermal diffusivity of nanofluids by considering the spherical as well as cylindrical-shaped nanoparticles using transient technique and predicted that Hamilton and Crosser models provide the best approximation for these thermophysical characteristics. Later on, Timofeeva et al. [28] theoretically explained the effect of the nanoparticle shape on thermophysical behaviour of alumina with the help of experimental data. Yang and Ma [29] provided the computer simulation for the understanding of translocation processes of nanoparticles with the usages of different shapes (ellipsoids, discs, rods, and spheres) of nanoparticles across a lipid bilayer. Maheshwary et al. [30] experimentally discussed the significance of the particle shape, particle size, and concentration on thermal conductivity of water-conveying titania nanofluid and predicted that thermal conductivity of the mixture is improved by intensifying the choices of the particle shape, size, and concentration. Sheikholeslami [31] discussed the effect of various shapes (platelet, brick, cylinder, and sphere) of nanoparticles on the forced convective flow of water-conveying cupric oxide nanofluid within a permeable lid-driven enclosure in the magnetic environment by using CVFEM and indicated that the Nusselt number declines with the augments of the Lorentz force. Rashid and Liang [32] numerically investigated the implication of the nanoparticle shape (sphere and lamina) on the dynamics of magnetized nanofluid with heat transference phenomenon, thermal radiation effect, and joule heating process towards an expanding disk through a porous space in a rotating frame. Dinarvand and Rostami [33] analyzed the shape factor influence of nanoparticles (graphene oxide and magnetite) for bidirectional unsteady dynamics of water-conveying hybrid nanofluid squeezed between two parallel surfaces using the Tiwari-Das model and predicted that the shape factor effect of nanoparticles has a crucial role in food processing, polymer processing, injection modeling, lubrication, etc. Bhattad and Sarkar [34] theoretically examined the significances of the nanoparticle size and shapes (brick, platelet, sphere, and cylinder) on the thermohydraulic enactment of a sheet evaporator by using hybrid nanofluids having various combinations of mixtures.

The combined significances of thermal radiation and Lorentz force space contribute a vital role in the development of combustion processes, nuclear weapons, electron ramifications, polarization process, stellar evolution, heat conduction process, petroleum reservoirs, etc. Turkyilmazoglu and Pop [35] numerically addressed the natural convection dynamics of radiative water-conveying nanofluid containing copper, alumina, titania, cupric oxide, and silver nanoparticles across a flat device. Devi and Devi [36] numerically examined the

effects of Newtonian heating and Lorentz force on bidirectional dynamics of water-conveying hybrid nanofluid with the mixture of copper and alumina. From this exploration, it is conveyed that hybrid nanofluid provides the better rate of heat transference than conventional nanofluid. Sheikholeslami and Sadoughi [37] numerically disclosed the MHD effect on the flow of nanofluid inside a porous enclosure with four square heat sources by considering the importance of nanoparticle shapes. Hayat et al. [38] discussed the radiative and heat transfer characteristics for hybrid mixture of silver and cupric oxide nanoparticles with water as base liquid in a rotating frame. It is deduced that rotation and radiation phenomena boost the thermal environment of the hybrid mixture. Some more recent exploration regarding the implications of the Lorentz force and porous media is found in the refs. [39–43].

The variation in the temperature fluctuation at the geometric surfaces is beneficial for several industrial and engineering applications. Liu and Andersson [44] implemented the variable thermal conditions to investigate the heat transference characteristics for 3D dynamics of a liquid towards a bidirectional expanding device. Both the heating processes, namely, PST (prescribed surface temperature) and PHF (prescribed heat flux), have been discussed by Liu and Andersson, and it was predicted that variable thermal conditions provide an improved rate of heat transference than arbitrary thermal conditions at the geometric surface. Oliveira et al. [45] discussed the practical applications of variable thermal conditions in the engineering processes like power converters, motor controllers, passive thermosyphons, and air conditioning process. Waini et al. [46] discussed the heat transference characteristic for the steady dynamics of hybrid nanofluid past a vertical thin needle by considering the variable heat flux at the geometric surface. Waini et al. [47] also investigated the heat transference process along with variable heat flux for the stagnated dynamics of hybrid nanofluid (alumina and copper) with water as working liquid on a contracting cylindrical geometry. Some more recent contributions related to the variable temperature of the geometrical surfaces are found in the refs. [48–52].

In the view of abovementioned comprehensive literature survey, it is noticed that much attention has not been given to the dynamics of hybrid nanofluid towards bidirectional elongating geometry. The main theme of the present contribution is to predict the effects of cylindrical-shaped nanoparticles (alumina and titania) for radiative water-conveying hybrid nanofluid flow towards an unsteady bidirectional elongating device with prescribed thermal conditions, and this type of contribution is not found in literature to the best of the author's knowledge. Additionally, influence of the Lorentz force is also incorporated in the mathematical model. Suitable mathematical relations have been used to transform the transport equations into dimensionless forms, and then, computer simulation is made via the Keller-Box method [53–59]. Finally, the foremost outcomes obtained through present numerical investigation are presented through various plots and tables.

2. Mathematical Formulation

In order to frame the unsteady mathematical model for bidirectional dynamics of water-conveying hybrid nanofluid with cylindrical-shaped nanoparticles (alumina (Al_2O_3) and titania (TiO_2)), the Cartesian configuration is adopted. The mathematical relation of the Lorentz force is used to inspect the MHD (magnetohydrodynamics) effects with strength $B_0 = b_0/\sqrt{1-ct}$ (b_0 represents the initial strength of the magnetic field). The mathematical relation of Rosseland approximation is then followed to examine the effects of thermal radiation. The tiny particles are considered in thermal equilibrium. The no-slip phenomenon is considered at the surface to keep the flow incompressible as well as laminar. Expansion velocity $u_w = ax/(1-ct)\,; a > 0, c > 0$ is opted along the x-axis, and the expansion velocity $v_w = by/(1-ct)\,; b \geq 0$ is decided along the y-axis, whereas $0 < z < \infty$ is the region covered by the hybrid nanofluid (as sketched in Figure 1). In order to provide the variable temperature mechanism at the surface, two types of thermal conditions, namely, PST and PHF, are applied. Table 1 is constructed to summarize the thermophysical characteristics of water H_2O, alumina, and titania.

In the continuation of the abovementioned assumptions with a boundary layer theory, the transport equations are manifested as follows (refs. [38, 52]):

$$\begin{aligned}
&\frac{\partial u}{\partial x} + \frac{\partial v}{\partial y} + \frac{\partial w}{\partial z} = 0,\\
&\frac{\partial u}{\partial t} + u\frac{\partial u}{\partial x} + v\frac{\partial u}{\partial y} + w\frac{\partial u}{\partial z} = \frac{\mu_{\mathrm{hnf}}}{\rho_{\mathrm{hnf}}}\frac{\partial^2 u}{\partial z^2} - \frac{\sigma_{\mathrm{hnf}}}{\rho_{\mathrm{hnf}}}{B_0}^2 u,\\
&\frac{\partial v}{\partial t} + u\frac{\partial v}{\partial x} + v\frac{\partial v}{\partial y} + w\frac{\partial v}{\partial z} = \frac{\mu_{\mathrm{hnf}}}{\rho_{\mathrm{hnf}}}\frac{\partial^2 v}{\partial z^2} - \frac{\sigma_{\mathrm{hnf}}}{\rho_{\mathrm{hnf}}}{B_0}^2 v,\\
&\frac{\partial T}{\partial t} + u\frac{\partial T}{\partial x} + v\frac{\partial T}{\partial y} + w\frac{\partial T}{\partial z} = \alpha_{\mathrm{hnf}}\frac{\partial^2 T}{\partial z^2} - \frac{1}{\left(\rho C_p\right)_{\mathrm{hnf}}}\frac{\partial q_{\mathrm{rad}}}{\partial z}.
\end{aligned} \tag{1}$$

The velocity and thermal conditions for equation (1) are conveyed as follows (ref. [41]):

$$\begin{aligned}
&z = 0 : u = u_w(x,t) = \frac{ax}{1-ct},\\
&v = v_w(y,t) = \frac{by}{1-ct},\\
&w = 0,\\
&z \longrightarrow \infty : u \longrightarrow 0,\\
&v \longrightarrow 0,\\
&\text{PST case} : z = 0 : T = T_w(x,y,t) = T_\infty + T_0\left(\frac{x^r y^s}{1-ct}\right),\\
&z \longrightarrow \infty : T \longrightarrow T_\infty,\\
&\text{PHF case} : z = 0 : -k_{\mathrm{hnf}}\left(\frac{\partial T}{\partial z}\right)_w = q_w(x,y,t) = T_1\left(\frac{x^r y^s}{1-ct}\right),\\
&z \longrightarrow \infty : T \longrightarrow T_\infty.
\end{aligned} \tag{2}$$

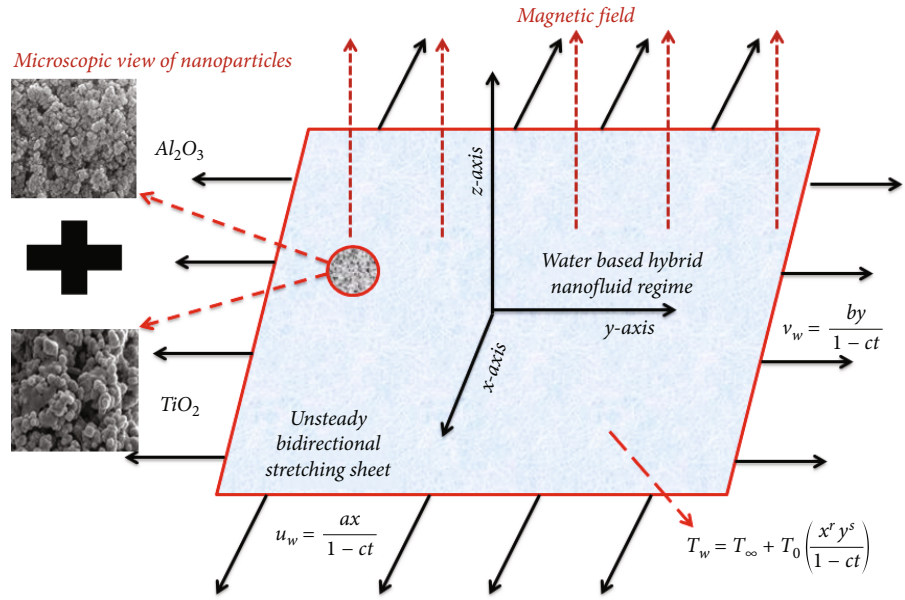

Figure 1: Graphical abstract of the considered hybrid nanofluid model.

Table 1: Thermophysical features of water, alumina, and titania nanoparticles (refs. [15, 17, 18]).

Thermophysical features	Base fluid	Nanoparticles	
	H_2O	$Al_2O_3(\psi_1)$	$TiO_2(\psi_2)$
Density (ρ): kg/m^3	997.1	3970	4250
Thermal conductivity (k): W/mK	0.613	40.0	8.9538
Specific heat (C_p): J/kgK	4179	765	686.2
Electrical conductivity: (σ): S/m	5.5×10^{-6}	35×10^6	0.24×10^7
Prandtl number: Pr	6.20	—	—

Here, (u, v, w) designates the velocity components along the x-, y-, and z-directions, respectively, T shows the temperature at the surface, time factor is symbolized by t, (r, s) are the indices that are used to control the temperature at the surface, T_0 and T_1 are dimensional constants, μ_{hnf} is opted to describe the effective viscosity of the hybrid mixture, ρ_{hnf} is chosen to label the density of the hybrid mixture, k_{hnf} is taken to mark the thermal conductivity of the hybrid mixture, $\alpha_{\text{hnf}} = k_{\text{hnf}}/(\rho C_p)_{\text{hnf}}$ is picked to state the thermal diffusivity of the hybrid mixture, $C_{p_{\text{hnf}}}$ is selected to represent the specific heat capacity, and σ_{hnf} is typified to express the influence of electrical conductivity of the hybrid nanofluid.

The mathematical relations to introduce the cylindrical shaped nanoparticles for present evolution of hybrid nanomaterial are composed as follows (refs. [2, 27, 31]):

$$\rho_{\text{hnf}} = \psi_1\rho_{p1} + \psi_2\rho_{p2} + (1-\psi_1-\psi_2)\rho_f,$$

$$(\rho C_p)_{\text{hnf}} = \psi_1(\rho C_p)_{p1} + \psi_2(\rho C_p)_{p2} + (1-\psi_1-\psi_2)(\rho C_p)_f,$$

$$\frac{k_{\text{hnf}}}{k_{\text{bf}}} = \frac{(k_{p2}+3.82k_{\text{bf}}) - 3.82\psi_2(k_{p2}-k_{\text{bf}})}{(k_{p2}+3.82k_{\text{bf}}) + \psi_2(k_{p2}-k_{\text{bf}})},$$

$$\frac{k_{\text{bf}}}{k_f} = \frac{(k_{p1}+3.82k_f) - 3.82\psi_1(k_{p1}-k_f)}{(k_{p1}+3.82k_f) + \psi_1(k_{p1}-k_f)},$$

$$\frac{\sigma_{\text{hnf}}}{\sigma_{\text{bf}}} = 1 + \frac{3\left((\sigma_{p2}/\sigma_{\text{bf}})-1\right)\psi_2}{(\sigma p_2/\sigma_{\text{bf}}) + 2 - \left((\sigma_{p2}/\sigma_{\text{bf}})-1\right)\psi_2},$$

$$\frac{\sigma_{\text{bf}}}{\sigma_f} = 1 + \frac{3\left((\sigma_{p1}/\sigma_f)-1\right)\psi_1}{(\sigma_{p1}/\sigma_f) + 2 - \left((\sigma_{p1}/\sigma_f)-1\right)\psi_1},$$

$$\alpha_{\text{hnf}} = \frac{k_{\text{hnf}}}{(\rho C_p)_{\text{hnf}}},$$

$$\frac{\mu_{\text{hnf}}}{\mu_{\text{bf}}} = 1 + 13.5\psi_2 + 904.4{\psi_2}^2,$$

$$\frac{\mu_{\text{bf}}}{\mu_f} = 1 + 13.5\psi_1 + 904.4{\psi_1}^2. \quad (3)$$

Here, quantities of volume fractions for alumina and titania nanoparticles are expressed through ψ_1 and ψ_2, respectively. The case of conventional fluid can be recovered by considering $\psi_1 = \psi_2 = 0$.

The equation for radiative heat transfer is defined as follows (refs. [35, 38]):

$$q_{\text{rad}} = -\frac{16\sigma^*}{3k^*} T_\infty{}^3 \frac{\partial T}{\partial z}. \tag{4}$$

Here, q_{rad} describes the radiative heat transference, σ^* illustrates the Stefan Boltzmann factor, and k^* explains the effect of the mean absorption factor.

The set of relations used to nondimensionalize the present mathematical model is conveyed as follows (refs. [41, 52]):

$$\begin{aligned} u &= \frac{ax}{1-ct} f'(\eta), \\ v &= \frac{ay}{1-ct} g'(\eta), \\ w &= -\left(\frac{a\vartheta_f}{1-ct}\right)^{1/2} [f(\eta) + g(\eta)], \\ \eta &= \left(\frac{a}{\vartheta_f(1-ct)}\right)^{1/2} z, \end{aligned} \tag{5}$$

$$\begin{aligned} \text{PST case} &: \theta(\eta) = \frac{T(x,y,z,t) - T_\infty}{T_w(x,y,t) - T_\infty}, \\ \text{PHF case} &: T - T_\infty = \frac{T_1}{k_f}\left(\frac{\vartheta_f}{a(1-ct)}\right)^{1/2} x^r y^s \phi(\eta). \end{aligned} \tag{6}$$

With the involvement of equations (6) and (7), the transport equations become

$$\varepsilon_1 f''' - f'^2 + (f+g)f'' - S\left(f' + \frac{\eta}{2} f''\right) - \varepsilon_2 M^2 f' = 0, \tag{7}$$

$$\varepsilon_1 g''' - g'^2 + (f+g)g'' - S\left(g' + \frac{\eta}{2} g''\right) - \varepsilon_2 M^2 g' = 0, \tag{8}$$

$$\text{PST case} : \varepsilon_3(1+R_d)\theta'' + \Pr\left((f+g)\theta' - \left(rf' + sg'\right)\theta - S\left(\theta + \frac{\eta}{2}\theta'\right)\right) = 0, \tag{9}$$

$$\text{PHF case} : \varepsilon_3(1+R_d)\phi'' + \Pr\left((f+g)\phi' - \left(rf' + sg'\right)\phi - S\left(\phi + \frac{\eta}{2}\phi'\right)\right) = 0, \tag{10}$$

with boundary restrictions

$$\begin{aligned} f(0) + g(0) &= 0, \\ f'(0) &= 1, \\ g'(0) &= \alpha, \\ f'(\infty) &\longrightarrow 0, \\ g'(\infty) &\longrightarrow 0, \\ \text{PST case} &: \theta(0) = 1, \\ \theta(\infty) &\longrightarrow 0, \\ \text{PHF case} &: \phi'(0) = -\frac{k_f}{k_{\text{hnf}}}, \phi(\infty) \longrightarrow 0. \end{aligned} \tag{11}$$

Here, the Hartmann number is recognized by $M = (\sigma_f/a\rho_f)^{1/2} b_0$, the unsteady factor is stated by $S = c/a$, the elongation ratio is expressed by $\alpha = b/a$, the Prandtl factor is indicated by $\Pr = \upsilon_f/\alpha_f$, $R_d = (16\sigma^*/3k^*k_f)T_\infty{}^3$ is the radiation factor, and $(\varepsilon_1, \varepsilon_2, \varepsilon_3)$ are the relations for the present hybrid mixture and these relations are elaborated as follows:

$$\begin{aligned} \varepsilon_1 &= \frac{\left(1 + 13.5\psi_2 + 904.4\psi_2{}^2\right)\left(1 + 13.5\psi_1 + 904.4\psi_1{}^2\right)}{\left(\psi_1\left(\rho_{p1}/\rho_f\right) + \psi_2\left(\rho_{p2}/\rho_f\right) + (1-\psi_1-\psi_2)\right)}, \\ \varepsilon_2 &= \frac{\left(1 + \left(\left(3\left(\left(\sigma_{p2}/\sigma_{\text{bf}}\right) - 1\right)\psi_2\right)/\left(\left(\sigma_{p2}/\sigma_{\text{bf}}\right) + 2 - \left(\left(\sigma_{p2}/\sigma_{\text{bf}}\right) - 1\right)\psi_2\right)\right)\right)\left(1 + \left(\left(3\left(\left(\sigma_{p1}/\sigma_f\right) - 1\right)\psi_1\right)/\left(\left(\sigma_{p1}/\sigma_f\right) + 2 - \left(\left(\sigma_{p1}/\sigma_f\right) - 1\right)\psi_1\right)\right)\right)}{\psi_1\left(\rho_{p1}/\rho_f\right) + \psi_2\left(\rho_{p2}/\rho_f\right) + (1-\psi_1-\psi_2)}, \\ \varepsilon_3 &= \frac{\left(\left(\left(k_{p2} + 3.82k_{\text{bf}}\right) - 3.82\psi_2\left(k_{p2} - k_{\text{bf}}\right)\right)/\left(\left(k_{p2} + 3.82k_{\text{bf}}\right) + \psi_2\left(k_{p2} - k_{\text{bf}}\right)\right)\right)\left(\left(\left(k_{p1} + 3.82k_f\right) - 3.82\psi_1\left(k_{p1} - k_f\right)\right)/\left(\left(k_{p1} + 3.82k_f\right) + \psi_1\left(k_{p1} - k_f\right)\right)\right)}{\psi_1\left(\left(\rho C_p\right)_{p1}/\left(\rho C_p\right)_f\right) + \psi_2\left(\left(\rho C_p\right)_{p2}/\left(\rho C_p\right)_f\right) + (1-\psi_1-\psi_2)}. \end{aligned} \tag{12}$$

The most fascinating quantities for thermal processes and most used in the improvement of heat exchanger devices are termed as skin-friction coefficients (i.e., C_{fx} and C_{fy}) and the local Nusselt number (i.e., Nu_x). The

mathematical formulations of these quantities are communicated as follows (refs. [36, 44, 51]):

$$
\begin{aligned}
C_{fx} &= \frac{\tau_{wx}}{\rho_f {u_w}^2},\\
C_{fy} &= \frac{\tau_{wy}}{\rho_f {v_w}^2},\\
\tau_{wx} &= \mu_{\mathrm{hnf}}\left(\frac{\partial u}{\partial z}\right)_{z=0},\\
\tau_{wy} &= \mu_{\mathrm{hnf}}\left(\frac{\partial v}{\partial z}\right)_{z=0},\\
\text{PST case}: Nu_x &= \frac{x q_h}{k_f(T_w - T_\infty)},\\
q_h &= -k_{\mathrm{hnf}}\left(\frac{\partial T}{\partial z}\right)_{z=0} + (q_{\mathrm{rad}})_w,\\
\text{PHF case}: Nu_x &= \frac{x q_h}{k_f(T - T_\infty)},\\
q_h &= -k_{\mathrm{hnf}}\left(\frac{\partial T}{\partial z}\right)_{z=0} + (q_{\mathrm{rad}})_w.
\end{aligned}
\tag{13}
$$

The dimensionless formulations of the abovementioned quantities using Reynold's numbers $\mathrm{Re}_x = x u_w/\vartheta_f$, $\mathrm{Re}_y = y v_w/\vartheta_f$ are transported as follows:

$$
\begin{aligned}
{\mathrm{Re}_x}^{1/2} C_{fx} = {} & \left(1 + 13.5\psi_1 + 904.4{\psi_1}^2\right)\\
& \cdot \left(1 + 13.5\psi_2 + 904.4{\psi_2}^2\right) f''(0),
\end{aligned}
\tag{14}
$$

$$
\begin{aligned}
{\mathrm{Re}_y}^{1/2} C_{fy} = {} & \alpha^{-3/2}\left(1 + 13.5\psi_1 + 904.4{\psi_1}^2\right)\\
& \cdot \left(1 + 13.5\psi_2 + 904.4{\psi_2}^2\right) g''(0),
\end{aligned}
\tag{15}
$$

$$
{\mathrm{Re}_x}^{-1/2} Nu_x = \begin{cases} -\dfrac{k_{\mathrm{hnf}}}{k_f}(1 + R_d)\theta'(0) & (\text{PST case}),\\[2ex] (1 + R_d)\dfrac{1}{\phi(0)} & (\text{PHF case}). \end{cases}
\tag{16}
$$

3. Keller-Box Simulation

The final form of the system of equations obtained through the aforementioned modeling along with boundary conditions is simulated via the Keller-Box approach. This numerical approach has accuracy of up to second order and has rapid convergence ability than other routine work numerical approaches (shooting method, RK-method, BVP4c, etc.). This approach also provides the flexibility about adoption of the step size for the computational domain and is more appropriate for the solution of boundary layer flow problems. The major advantage of this method over other numerical methods is its unique conversion procedure of differential equations into algebraic equations using central difference approximations. Foremost steps to implement this numerical approach are stated below and summarized via the flow chart (Figure 2):

(i) The first step is to transform the higher-order differential equations into first-order differential equations

(ii) The next step is to transmute the obtained differential system into the difference equation system via central difference numerical approximations

(iii) Linearization of the system of difference equations is completed with the courtesy of Newton's linearization standard method

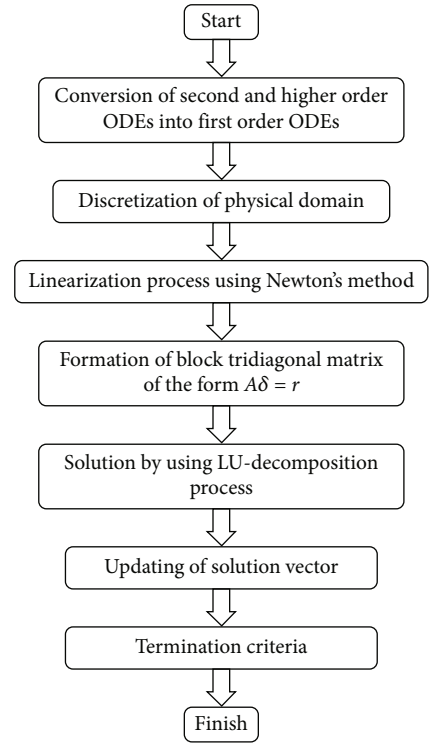

Figure 2: Flow chart of numerical procedure.

Table 2: Convergence of the Keller-Box simulation for $\alpha = S = M = 0.5$, $r = s = 1.0$, $\psi_1 = \psi_2 = 0.04$, $R_d = 0.5$.

n_p	$-f''(0)$	$-g''(0)$	$-\theta'(0)$	$1/\phi(0)$
500	0.6718217	0.317969	2.631693	3.556174
1000	0.6718218	0.317969	2.631367	3.555733
1500	0.6718218	0.317969	2.631306	3.555651
2000	0.6718218	0.317969	2.631285	3.555623
2500	0.6718218	0.317969	2.631275	3.555609
3000	0.6718218	0.317969	2.63127	3.555602
3500	0.6718218	0.317969	2.631267	3.555598
4000	0.6718218	0.317969	2.631265	3.555595
4500	0.6718218	0.317969	2.631263	3.555593
5000	0.6718218	0.317969	2.631262	3.555592
10000	0.6718218	0.317969	2.631262	3.555592

Table 3: Outcomes in the nonappearance of nanoparticles, magnetic and unsteadiness aspects.

$\alpha = 1.0$	$-f''(0)$	$f(\infty)$	$-g''(0)$	$g(\infty)$
Present	1.173722	0.751498	1.173722	0.751498
Liu and Andersson [44]	1.173721	0.751494	1.173721	0.751494
$\alpha = 0.5$	$-f''(0)$	$f(\infty)$	$-g''(0)$	$g(\infty)$
Present	1.093095	0.842387	0.465205	0.451678
Liu and Andersson [44]	1.093096	0.842360	0.465206	0.451663
$\alpha = 0.0$	$-f''(0)$	$f(\infty)$	$-g''(0)$	$g(\infty)$
Present	−1.0	1.0	0.0	0.0
Liu and Andersson [44]	−1.0	1.0	0.0	0.0

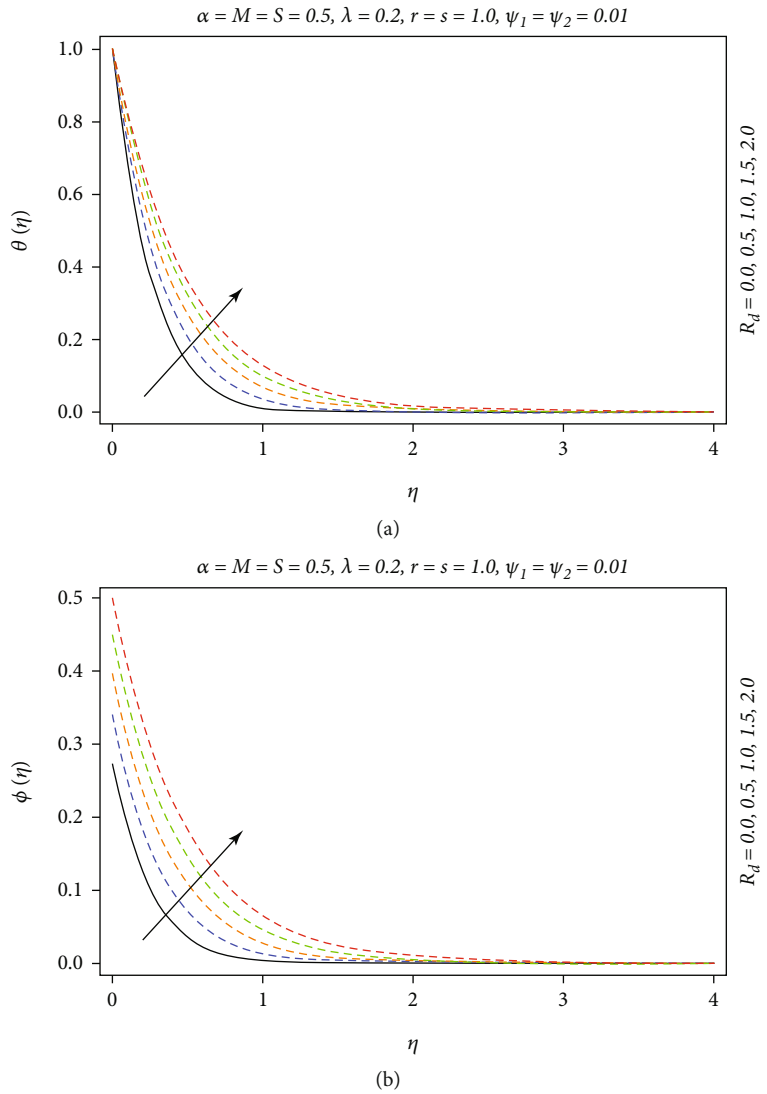

Figure 3: (a, b) Temperature fluctuation against the variation of radiation factor R_d for the PST case and for the PHF case.

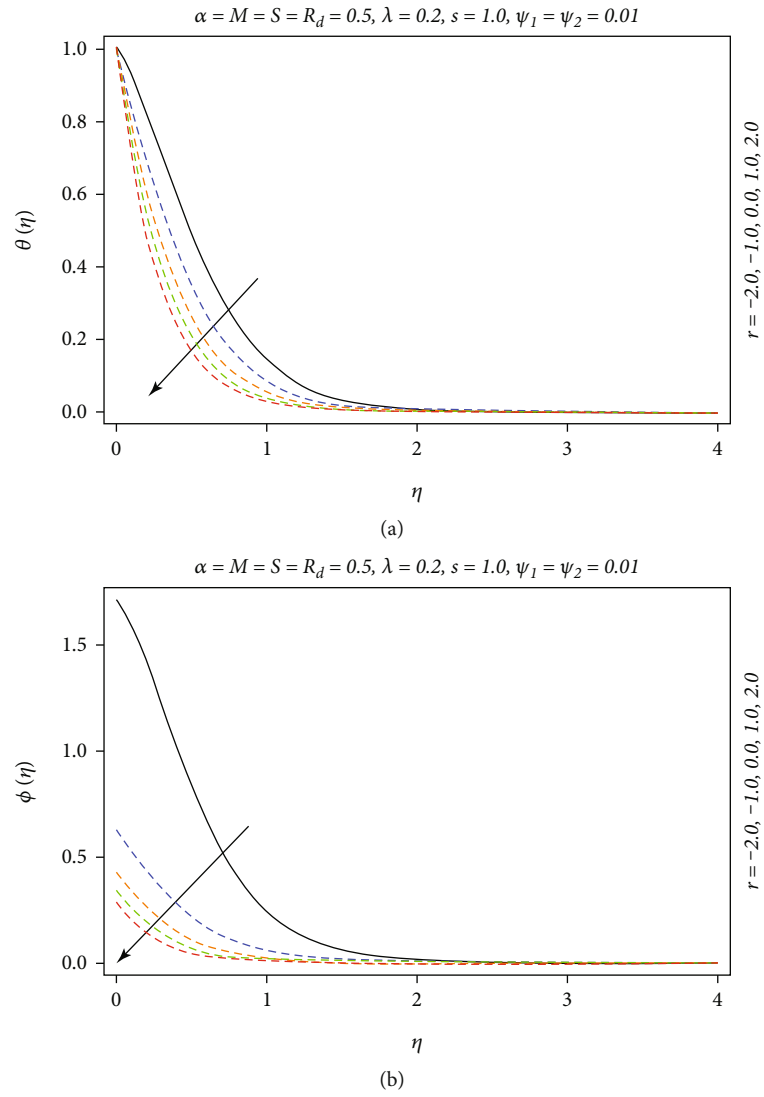

Figure 4: (a, b) Temperature fluctuation against the variation of the index r for the PST case and for the PHF case.

(iv) The linearized equations are then arranged into matrix-vector forms

(v) The LU decomposition technique is opted to solve the obtained matrix-vector problem

(vi) Finally, the value of the unknown vector provides the numerical solution of the aforementioned mathematical problem

During the implementation of the abovementioned steps, the computational domain $[0\infty)$ is truncated into the finite domain $[\eta_0\, \eta_\infty]$. In order to obtain the first approximation of the numerical solution, we selected $\eta_0 = 0, \eta_\infty = 20$, $n_p = 500, h = (\eta_\infty - \eta_0)/n_p$, and then, the desired accuracy, i.e., $\varepsilon = 10^{-6}$, is achieved by varying the value of n_p (the numbers of grid points) with the reduction in the value of h (step size).

Table 2 is designed to estimate the rate of convergence of the Keller-Box simulation as well as to find the best choice of n_p for the simulation of the local Nusselt number and skin-friction coefficients. It is deduced through Table 2 that one thousand grid points are enough for the convergent solution of $f''(0)$ and five hundred grid points are sufficient to achieve the convergence criteria for $g''(0)$, whereas five thousand grid points are necessary to attain the convergent approximation for both $\theta'(0)$ as well as $1/\phi(0)$. In order to check the stability of the Keller-Box solution, the value of n_p is increased up to ten thousand and the solution is found consistent. The convergent solution obtained through Table 2 is used for further manipulations in order to find the impact of involved parameters on the thermal setup, local Nusselt number, and skin-friction coefficients.

4. Code Validation

In order to validate the numeric code for the solution of the considered problem, the outfalls reported in the present contribution have been compared with the outfalls discussed in

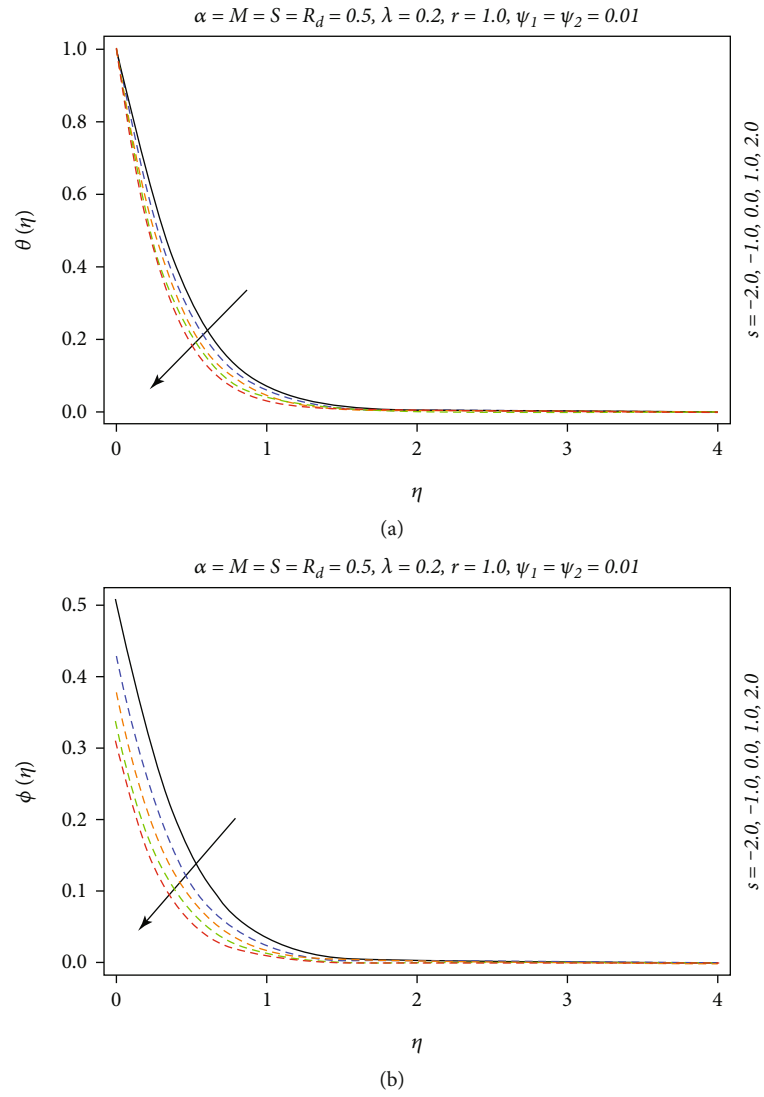

Figure 5: (a, b) Temperature fluctuation against the variation of the index s for the PST case and for the PHF case.

the article (Liu and Andersson [44]) for $f''(0), g''(0), f(\infty)$ and $g(\infty)$ in the absence of nanoparticles. A convincing scientific connection has been found between the present scrutiny and the published activity. In this regard, Table 3 is arranged in the analysis.

5. Results and Discussion

The present heading describes the importance of the involved important parameters like radiation factor R_d and temperature maintaining indices (r, s) on thermal setups $[\theta(\eta), \phi(\eta)]$ via various plots, whereas the physical quantities like the local Nusselt number and skin friction coefficients are discussed for various estimations of involved constraints via various graphs and tables. Moreover, the thermophysical properties for the present hybrid mixture are also computed at the end of this section and discussed deeply. Figure 3 describes the impact of radiation factor R_d on $\theta(\eta)$ and on $\phi(\eta)$. It is detected through Figures 3(a) and 3(b) that the escalating choice of R_d enhances the worth of thermal setups. The thickness of the thermal layer is observed larger for smaller choices of R_d as compared to larger estimations of R_d. The maximum temperature for the PST mechanism is observed as one, whereas the maximum temperature for the PHF case is noticed as 0.5 when R_d is increased from 0 to 2.0. Overall, the strength of the thermal setup for the PHF case is observed to be more prominent than that for the PST case. Physically, the abovementioned changes are produced because R_d is the mathematical ratio of Stefan Boltzman number σ^* to mean absorption factor k^*. The value of σ^* is increased whereas the value of k^* is diminished with the positive tendency of R_d. Figure 4 explains the influence of temperature maintaining index r corresponding to the x-direction on $\theta(\eta)$ and on $\phi(\eta)$ while other parameters are being fixed. The temperature of hybrid nanofluid is diminished for both the PST and PHF cases with the escalating amount of r. The value of temperature is detected higher for the PHF case than the PST case for $r \leq -2$ and is deduced

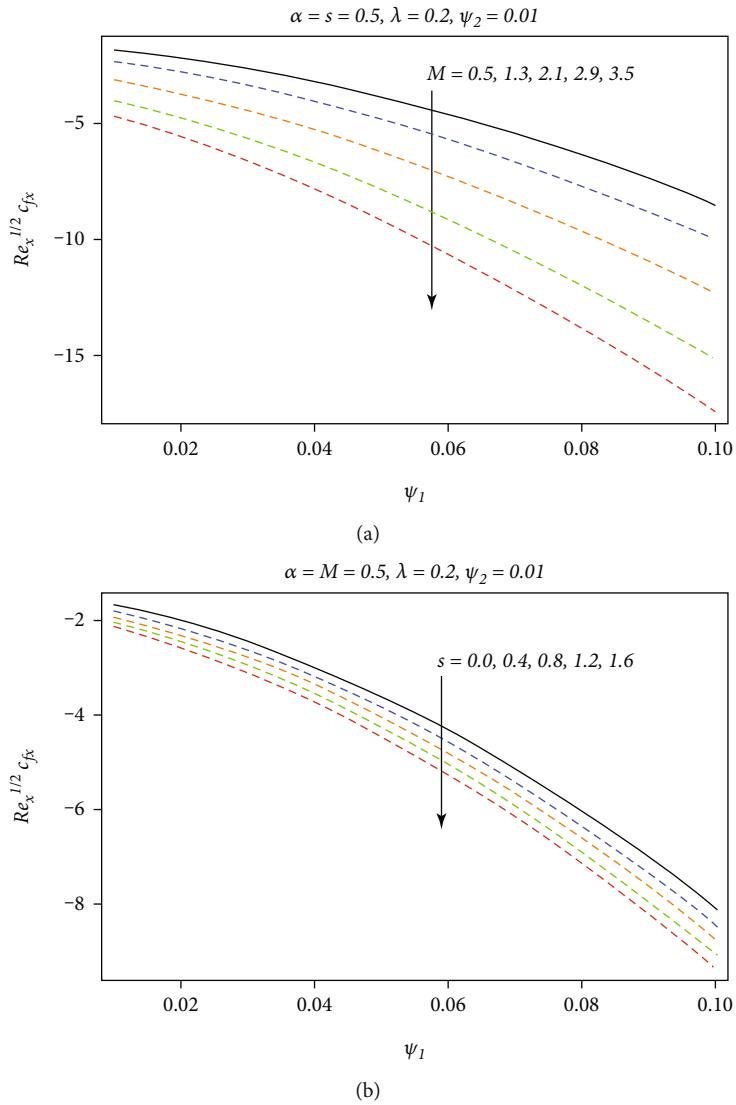

FIGURE 6: (a, b) Skin-friction coefficient C_{fx} against the variations in ψ_1&M and ψ_1&S.

higher for the PST case than the PHF case for other choices of r. Physically, the temperature distribution is well dominant for variable thermal conditions than arbitrary thermal conditions. The wideness of the thermal layer is larger in the PHF case than the PST case. Figure 5 is plotted to explain the worth of temperature maintaining index s corresponding to the y-direction on $\theta(\eta)$ and on $\phi(\eta)$ by keeping the other involved factors fixed. The temperature with the higher estimations of s is reduced for both the PHF and PST mechanisms. The value of temperature fluctuation is attained higher for PST conditions than PHF conditions for all the choices of s, but the thermal thickness is achieved quite dominant for the PHF case as associated with the PST case.

Figure 6(a) manifests the combined influence of ψ_1 and M on C_{fx} for fixed values of other involved parameters. Skin-friction coefficient C_{fx} is reduced with increasing amounts of both M and ψ_1. Physically, more electric conduction is produced in the flow of the hybrid mixture with the positive growth in M from 0.5 to 3.5. Skin-friction coefficient C_{fx} is reduced with the phenomenon of electric conduction. Moreover, the electrical conductivity of alumina is much higher than the electrical conductivity of host liquid and this phenomenon produces the reduction in the value of C_{fx}. The smaller selection of ψ_1 produces the stream of moderate thickness, whereas the thickness of the stream is observed to be double when ψ_1 reached 0.10. Figure 6(b) explains the combined influence of ψ_1 and S on C_{fx} for fixed selections of other involved constraints. Skin-friction coefficient C_{fx} is reduced with the higher estimation of S. Physically, expansion rate a is reduced with the improvement in the value of S, and therefore, reduction in the computation of C_{fx} is attained. Figure 7(a) reveals the collective effect of ψ_2 and λ on C_{fy} with other parameters being kept fixed. Skin-friction coefficient C_{fy} is abridged with growing amounts of both λ and ψ_2. Actually, a less elongation rate is produced with the development in λ from 0.2 to 1.4.

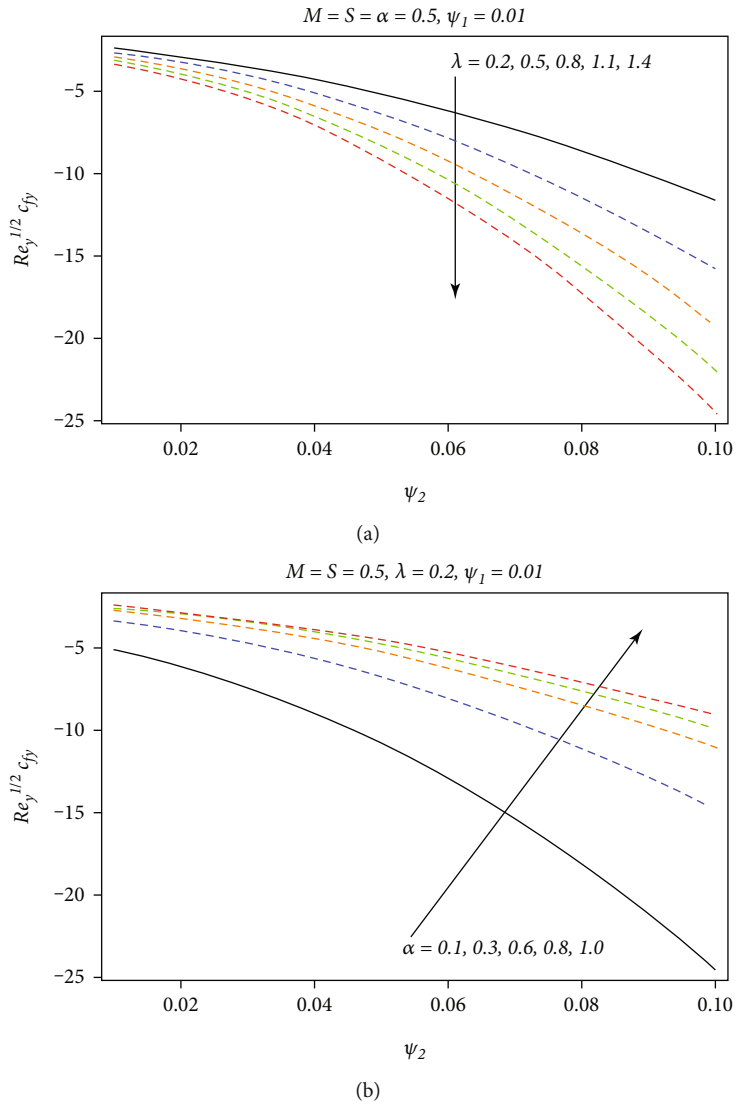

Figure 7: (a, b) Skin-friction coefficient C_{fy} against the variations in ψ_2&λ and ψ_2&α.

Skin-friction coefficient C_{fy} is diminished with the productions of a less elongation rate. Moreover, the electrical conductivity of titania is much higher than the electrical conductivity of host liquid and this phenomenon produces the reduction in the computation of C_{fy}. As electrical conductivity of titania is higher than the electrical conductivity of alumina, therefore, faster reduction in C_{fy} is achieved than C_{fx}. The smaller assortment of ψ_2 yields the stream of minute thickness, whereas the thickness of the stream is observed triple when ψ_2 reached 0.10. Figure 7(b) elucidates the joined impact of ψ_2 and α on C_{fy} for stationary values of other mathematical constraints. Skin-friction coefficient C_{fy} is enhanced with the advancement in α. Precisely, expansion rate b is enhanced and expansion rate a is diminished with the development in α, and therefore, enhancement in the computation of C_{fy} is attained.

Figure 8(a) explores the graphical assessment of Nusselt number Nu_x against the variations in R_d and r with other parameters being retained as fixed. Nusselt number Nu_x is improved with the enhancement in r from −2.0 to 2.0, and also, it is increased with the escalation in R_d from 0.0 to 2.0. Energy is transformed in the form of electromagnetic waves with the involvement of thermal radiation, and it is more efficient in porous space or vacuum because it is the ideal situation for full transmission of the radiation energy. The value of Nu_x is augmented with the escalation in R_d from 0.0 to 2.0. The rate of heat transference is observed slower for negative values of r than positive values of r because the surface temperature is mentioned higher for the negative value of r than the positive value of r, and therefore, the thermal flux across the surface will be higher for the positive value of r than its negative value. As a result, the Nusselt number Nu_x is tremendously improved.

Figure 8(b) describes the graphical evaluation of Nusselt number Nu_y against the variations in S and s with other parameters being taken as fixed. Nusselt number Nu_y is improved with the enhancement in s from −2.0 to 2.0, and

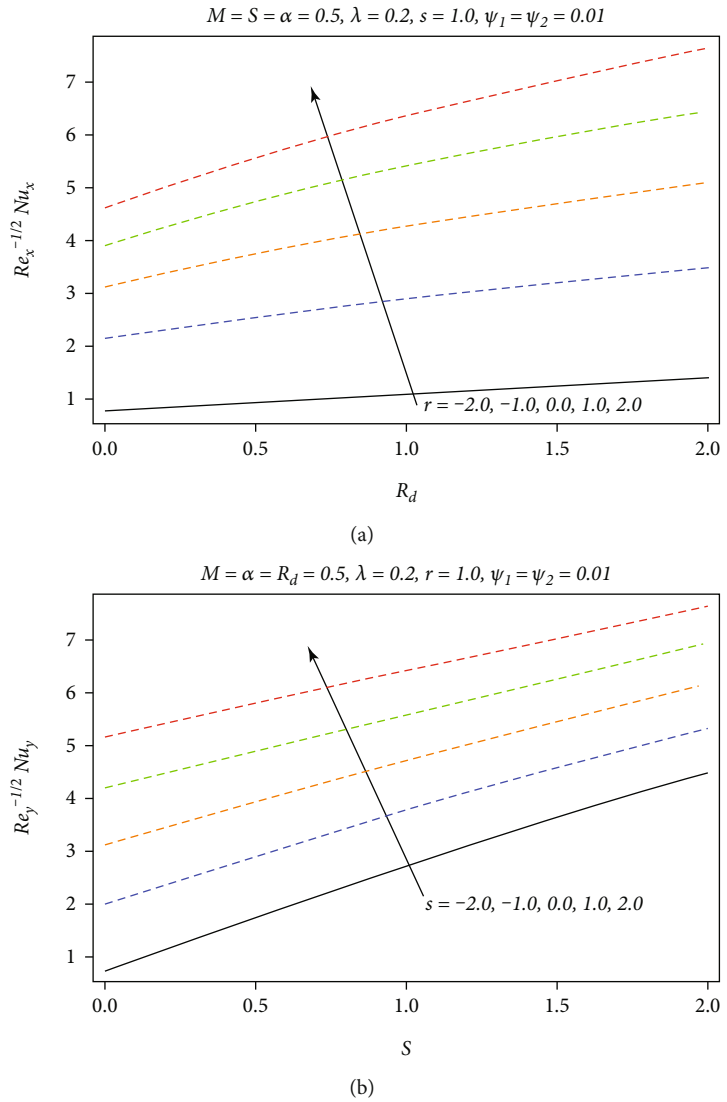

Figure 8: Nusselt number Nu_x against the variations in (a) R_d&r and Nu_y against the variations in (b) S&s.

Table 4: Contribution of solid volume fractions ψ_1 and ψ_2 on thermal interest quantities for $\alpha = S = M = 0.5, r = s = 1.0, R_d = 0.5$.

Nanoparticle volume fractions		$-\mathrm{Re}_y^{1/2} C_{fx}$	$-\mathrm{Re}_y^{1/2} C_{fy}$	$\left(\mathrm{Re}_x^{-1/2}/(1+R_d)\right) Nu_x$	
ψ_1	ψ_2			VST case	VHF case
0.01	0.01	1.818652	2.354086	3.165999	3.165999
0.04	0.01	3.199621	4.200442	3.392241	3.392241
0.07	0.01	5.443228	7.263307	3.584352	3.584352
0.10	0.01	8.510418	11.50723	3.751383	3.751383
0.13	0.01	12.42493	16.96354	3.903712	3.903712
0.16	0.01	17.20563	23.65449	4.046176	4.046176
0.01	0.04	3.207035	4.209267	3.351655	3.351655
0.01	0.07	5.46183	7.285107	3.50311	3.50311
0.01	0.10	8.542308	11.54414	3.630213	3.630213
0.01	0.13	12.47104	17.01642	3.743252	3.743252
0.01	0.16	17.26637	23.72367	3.846784	3.846784

Table 5: Fluctuations in the thermophysical behaviours for the existing hybrid mixture with $\psi_1 = 0.01$.

ψ_2	ρ_{hnf}	$(\rho C_p)_{\text{hnf}} \times 10^3$	k_{hnf}	$\sigma_{\text{hnf}} \times 10^{-6}$
0.00	1026.829	4.14486	0.6407428664	5.666667
0.01	1059.358	4.109932	0.6634263686	5.838384
0.03	1124.416	4.040076	0.7098079091	6.19244
0.05	1189.474	3.97022	0.7575933453	6.561404
0.07	1254.532	3.900364	0.8068473972	6.946237
0.09	1319.59	3.830508	0.8576388251	7.347985

Table 6: Fluctuations in the thermophysical behaviours for the existing hybrid mixture with $\psi_2 = 0.01$.

ψ_1	ρ_{hnf}	$(\rho C_p)_{\text{hnf}} \times 10^3$	k_{hnf}	$\sigma_{\text{hnf}} \times 10^{-6}$
0.00	1029.629	4.144072	0.6349801229	5.666667
0.01	1059.358	4.109932	0.6634263686	5.838384
0.03	1118.816	4.041652	0.7218911348	6.19244
0.05	1178.274	3.973372	0.7825545636	6.561404
0.07	1237.732	3.905092	0.8455479603	6.946237
0.09	1297.19	3.836812	0.9110132942	7.347985

also, it is increased with the escalation in S from 0.0 to 2.0. The transmission of heat is perceived slower for negative selections of s than positive selections of s because the stretching device is maintained at higher temperature for the negative value of s than the positive value of s, and therefore, thermal flux across the stretching device will be higher for the positive value of s than its negative value. As a result, the Nusselt number Nu_y is extremely enriched. Physically, unsteady expansion parameter S is involved in equation (9) with the sum of dimensionless temperature and its derivative with respect to η. As a result, the rate of heat transference across the yz plane is increased.

Roles of solid volume fractions ψ_1 for alumina and ψ_2 for titania on the local Nusselt number as well as on skin friction coefficients are discussed in Table 4. It is attained in Table 4 that escalating selections of ψ_1 and ψ_2 improve the skin-friction coefficients for the present model. It is also observed that the impact of ψ_1 and ψ_2 is more dominant for the flow along the y-direction as compared to the x-direction. Mathematically, the involvement of α is absent in equation (14), whereas it is involved in the reciprocal form as described in equation (15). As in our study, the value of α is selected to be 0.5, so the numerical value of $g''(0)$ is observed to be higher than the numerical value of $f''(0)$. Moreover, the roles of ψ_1 and ψ_2 on the local Nusselt number are also discussed in Table 3 and it is deduced that higher estimations of ψ_1 and ψ_2 in the range $[0.01\, 0.16]$ improve the rate of heat transference which is beneficial for many industrial and engineering applications. Furthermore, the rate of heat transference is observed to be equal quantitatively for both the PST and PHF mechanisms. The thermophysical features for the present hybrid mixture are discussed in Table 5 for various choices of ψ_2 (the weightage of titania) by adjusting $\psi_1 = 0.01$. The escalating estimation of ψ_2 enhances the density, thermal conductivity, and electrical conductivity of the hybrid mixture whereas the heat capacity is reduced with the present development in ψ_2. Physically, the mixture of alumina and titania with the working fluid, i.e., water, provides the improvement in the thermophysical features as compared to that in Table 1. In Table 6, thermophysical characteristics for present hybrid combination are computed for different selections of ψ_1 (the solid volume fraction of alumina) by taking $\psi_2 = 0.01$. With the increase of ψ_1, the density, the electrical conductivity, and the thermal conductivity are improved but the heat capacity is condensed with this variation. The base fluid, i.e., water, delivers enlargement in thermophysical properties of hybrid nanofluid associated to Table 1 with the chemically mixture of alumina and titania.

6. Conclusions

This study provides the mathematical analysis for unsteady bidirectional dynamics of radiative water-conveying hybrid nanofluid (i.e., the combination of titania and alumina) with the significance of variable thermal conditions (PST and PHF) and impact of the cylindrical shape of nanoparticles. The influence of the Lorentz force is also incorporated to make the investigation more impactful. Numerical simulation is made via the Keller-Box approach, and key observations are listed as follows:

(i) The thermophysical features of the hybrid nanofluid except specific heat are improved with the involvement of the cylindrical shape of nanoparticles, i.e., titania and alumina

(ii) The rate of heat transference is observed identical for both the PST and PHF cases

(iii) The magnitude of the stress applied on the y-direction is observed to be higher than the magnitude of the stress applied along the x-direction with the positive estimations of volume fractions of nanoparticles

(iv) The temperature of the hybrid nanofluid is increased with the development in the choice of R_d and decreased with the improvement in the choices of temperature maintaining indices (r, s)

(v) Skin-friction coefficients are reduced with progressions in the values of the Hartmann number, unsteady parameter, and volume percentages of nanoparticles

(vi) The local Nusselt number is improved with developments in the amounts of radiation and unsteady parameters

This scientific contribution has many mechanical, biomedical, and commercial applications. These are coating a sheet with hybrid nanomaterials, manufacturing of printing ink, degrading organic contaminants, manufacturing of sodium vapour lamps, etc. This study is also really helpful

for the researchers working in the field of nanomaterials and can be protracted in the future by considering different geometries.

Nomenclature

B_0: Strength of magnetic field
a, b: Stretching rates
t: Time
c: Time coefficient
x, y, z: Space coordinates
u_w, v_w: Stretching velocities
PST: Prescribed surface temperature
PHF: Prescribed heat flux
T_w: Surface temperature
r, s: Thermal indices
T_0, T_1: Dimensional constants
T_∞: Ambient temperature
u, v, w: Velocity field components
T: Temperature
hnf: Hybrid nanofluid
μ_{hnf}: Dynamic viscosity of hnf
ρ_{hnf}: Density of hnf
σ_{hnf}: Electrical conductivity of hnf
k_{hnf}: Thermal conductivity of hnf
α_{hnf}: Thermal diffusivity of hnf
$C_{p_{\text{hnf}}}$: Specific heat capacity of hnf
ψ_1: Volume fraction of alumina
ψ_2: Volume fraction of titania
f: Fluid
bf: Base fluid
$p1$: Alumina nanoparticles
$p2$: Titania nanoparticles
q_{rad}: Radiative heat transfer
σ^*: Stefan Boltzmann constant
k^*: Mean absorption coefficient
η: Similarity variable
f', g': Dimensionless velocities
θ, ϕ: Dimensionless temperatures
Pr: Prandtl number
R_d: Radiation parameter
S: Unsteady parameter
M: Hartmann number
$\varepsilon_1, \varepsilon_2, \varepsilon_3$: Dimensionless quantities
Re_x, Re_y: Reynolds numbers
Nu_x: Nusselt number
C_{fx}, C_{fy}: Skin friction coefficients
α: Stretching ratio parameter
ρ, k, C_p, σ: Thermophysical properties
h: Step size
ε: Convergence criterion
n_p: Numbers of grid points.

Data Availability

The raw data supporting the conclusion of this report will be made available by the corresponding author without undue reservation.

Conflicts of Interest

The authors declare that they have no competing interests.

Authors' Contributions

All authors contributed equally to this work, and all the authors have read and approved the final version of the report.

References

[1] J. C. Maxwell, *A Treatise on Electricity and Magnetism*, vol. 1, Clarendon Press, Oxford, 1873.

[2] R. L. Hamilton and O. K. Crosser, "Thermal conductivity of heterogeneous two-component systems," *Industrial & Engineering Chemistry Fundamentals*, vol. 1, no. 3, pp. 187–191, 1962.

[3] N. Masoumi, N. Sohrabi, and A. Behzadmehr, "A new model for calculating the effective viscosity of nanofluids," *Journal of Physics D: Applied Physics*, vol. 42, no. 5, article 055501, 2009.

[4] W. A. Khan and I. Pop, "Boundary-layer flow of a nanofluid past a stretching sheet," *International Journal of Heat and Mass Transfer*, vol. 53, no. 11-12, pp. 2477–2483, 2010.

[5] M. Sheikholeslami and H. B. Rokni, "Simulation of nanofluid heat transfer in presence of magnetic field: a review," *International Journal of Heat and Mass Transfer*, vol. 115, pp. 1203–1233, 2017.

[6] R. B. Ganvir, P. V. Walke, and V. M. Kriplani, "Heat transfer characteristics in nanofluid–a review," *Renewable and Sustainable Energy Reviews*, vol. 75, pp. 451–460, 2017.

[7] J. Sarkar, P. Ghosh, and A. Adil, "A review on hybrid nanofluids: recent research, development and applications," *Renewable and Sustainable Energy Reviews*, vol. 43, pp. 164–177, 2015.

[8] N. A. C. Sidik, M. M. Jamil, W. M. A. A. Japar, and I. M. Adamu, "A review on preparation methods, stability and applications of hybrid nanofluids," *Renewable and Sustainable Energy Reviews*, vol. 80, pp. 1112–1122, 2017.

[9] I. Waini, A. Ishak, and I. Pop, "Unsteady flow and heat transfer past a stretching/shrinking sheet in a hybrid nanofluid," *International Journal of Heat and Mass Transfer*, vol. 136, pp. 288–297, 2019.

[10] A. A. Minea, "Hybrid nanofluids based on Al_2O_3, TiO_2 and SiO_2: numerical evaluation of different approaches," *International Journal of Heat and Mass Transfer*, vol. 104, pp. 852–860, 2017.

[11] K. Y. Leong, Z. A. Najwa, K. K. Ahmad, and H. C. Ong, "Investigation on stability and optical properties of titanium dioxide and aluminum oxide water-based nanofluids," *International Journal of Thermophysics*, vol. 38, no. 5, p. 77, 2017.

[12] G. M. Moldoveanu, A. A. Minea, M. Iacob, C. Ibanescu, and M. Danu, "Experimental study on viscosity of stabilized Al_2O_3, TiO_2 nanofluids and their hybrid," *Thermochimica Acta*, vol. 659, pp. 203–212, 2018.

[13] G. M. Moldoveanu, A. A. Minea, G. Huminic, and A. Huminic, "Al2O3/TiO2 hybrid nanofluids thermal conductivity," *Journal of Thermal Analysis and Calorimetry*, vol. 137, no. 2, pp. 583–592, 2019.

[14] M. Shirazi, S. Kord, and Y. Tamsilian, "Novel smart water-based Titania nanofluid for enhanced oil recovery," *Journal of Molecular Liquids*, vol. 296, p. 112064, 2019.

[15] S. A. Khan, M. I. Khan, T. Hayat, M. F. Javed, and A. Alsaedi, "Mixed convective non-linear radiative flow with TiO2-cu-water hybrid nanomaterials and induced magnetic field," *International Journal of Numerical Methods for Heat & Fluid Flow*, vol. 29, no. 8, pp. 2754–2774, 2019.

[16] A. Asadi, I. M. Alarifi, and L. K. Foong, "An experimental study on characterization, stability and dynamic viscosity of CuO-TiO_2/water hybrid nanofluid," *Journal of Molecular Liquids*, vol. 307, p. 112987, 2020.

[17] S. Ahmad, K. Ali, M. Rizwan, and M. Ashraf, "Heat and mass transfer attributes of copper-aluminum oxide hybrid nanoparticles flow through a porous medium," *Case Studies in Thermal Engineering*, vol. 25, p. 100932, 2021.

[18] B. Ali, R. A. Naqvi, L. Ali, S. Abdal, and S. Hussain, "A comparative description on time-dependent rotating magnetic transport of a water base liquid H2O with hybrid nanomaterials Al2O3-Cu and Al2O3-TiO2 over an extending sheet using Buongiorno model: finite element approach," *Chinese Journal of Physics*, vol. 70, pp. 125–139, 2021.

[19] P. K. Kanti, K. V. Sharma, A. A. Minea, and V. Kesti, "Experimental and computational determination of heat transfer, entropy generation and pressure drop under turbulent flow in a tube with fly ash-Cu hybrid nanofluid," *International Journal of Thermal Sciences*, vol. 167, p. 107016, 2021.

[20] I. S. Okeke, K. K. Agwu, A. A. Ubachukwu, and F. I. Ezema, "Influence of transition metal doping on physiochemical and antibacterial properties of ZnO nanoparticles: a review," *Applied Surface Science Advances*, vol. 8, p. 100227, 2022.

[21] P. Sharma, Z. Said, S. Memon et al., "Comparative evaluation ofAI-based intelligentGEPandANFISmodels in prediction of thermophysical properties ofFe3O4-coatedMWCNThybrid nanofluids for potential application in energy systems," *International Journal of Energy Research*, 2022.

[22] A. K. Tiwari, V. Kumar, Z. Said, and H. K. Paliwal, "A review on the application of hybrid nanofluids for parabolic trough collector: recent progress and outlook," *Journal of Cleaner Production*, vol. 292, p. 126031, 2021.

[23] Z. Said, M. Ghodbane, L. S. Sundar, A. K. Tiwari, M. Sheikholeslami, and B. Boumeddane, "Heat transfer, entropy generation, economic and environmental analyses of linear fresnel reflector using novel rGO- Co_3O_4 hybrid nanofluids," *Renewable Energy*, vol. 165, pp. 420–437, 2021.

[24] F. Ali, K. Loganathan, S. Eswaramoorthi, K. Prabu, A. Zaib, and D. K. Chaudhary, "Heat Transfer Analysis on Carboxymethyl Cellulose Water-Based Cross Hybrid Nanofluid Flow with Entropy Generation," *Journal of Nanomaterials*, vol. 2022, Article ID 5252918, 11 pages, 2022.

[25] A. K. Tiwari, N. S. Pandya, Z. Said, H. F. Öztop, and N. Abu-Hamdeh, "4S consideration (synthesis, sonication, surfactant, stability) for the thermal conductivity of CeO2 with MWCNT and water based hybrid nanofluid: an experimental assessment," *Colloids and Surfaces A: Physicochemical and Engineering Aspects*, vol. 610, p. 125918, 2021.

[26] N. A. Zainal, R. Nazar, K. Naganthran, and I. Pop, "Unsteady three-dimensional MHD non-axisymmetric Homann stagnation point flow of a hybrid Nanofluid with stability analysis," *Mathematics*, vol. 8, no. 5, p. 784, 2020.

[27] X. Zhang, H. Gu, and M. Fujii, "Effective thermal conductivity and thermal diffusivity of nanofluids containing spherical and cylindrical nanoparticles," *Journal of Applied Physics*, vol. 100, no. 4, article 044325, 2006.

[28] E. V. Timofeeva, J. L. Routbort, and D. Singh, "Particle shape effects on thermophysical properties of alumina nanofluids," *Journal of Applied Physics*, vol. 106, no. 1, article 014304, 2009.

[29] K. Yang and Y. Q. Ma, "Computer simulation of the translocation of nanoparticles with different shapes across a lipid bilayer," *Nature Nanotechnology*, vol. 5, no. 8, pp. 579–583, 2010.

[30] P. B. Maheshwary, C. C. Handa, and K. R. Nemade, "A comprehensive study of effect of concentration, particle size and particle shape on thermal conductivity of titania/water based nanofluid," *Applied Thermal Engineering*, vol. 119, pp. 79–88, 2017.

[31] M. Sheikholeslami, "Magnetic field influence on CuO-H_2O nanofluid convective flow in a permeable cavity considering various shapes for nanoparticles," *International Journal of Hydrogen Energy*, vol. 42, no. 31, pp. 19611–19621, 2017.

[32] U. Rashid and H. Liang, "Investigation of nanoparticles shape effects on MHD nanofluid flow and heat transfer over a rotating stretching disk through porous medium," *International Journal of Numerical Methods for Heat & Fluid Flow*, vol. 30, no. 12, pp. 5169–5189, 2020.

[33] S. Dinarvand and M. N. Rostami, "Three-dimensional squeezed flow of aqueous magnetite–graphene oxide hybrid nanofluid: a novel hybridity model with analysis of shape factor effects," *Proceedings of the Institution of Mechanical Engineers, Part E: Journal of Process Mechanical Engineering*, vol. 234, no. 2, pp. 193–205, 2020.

[34] A. Bhattad and J. Sarkar, "Effects of nanoparticle shape and size on the thermohydraulic performance of plate evaporator using hybrid nanofluids," *Journal of Thermal Analysis and Calorimetry*, vol. 143, no. 1, pp. 767–779, 2021.

[35] M. Turkyilmazoglu and I. Pop, "Heat and mass transfer of unsteady natural convection flow of some nanofluids past a vertical infinite flat plate with radiation effect," *International Journal of Heat and Mass Transfer*, vol. 59, pp. 167–171, 2013.

[36] S. S. U. Devi and S. A. Devi, "Numerical investigation of three-dimensional hybrid cu–Al2O3/water nanofluid flow over a stretching sheet with effecting Lorentz force subject to Newtonian heating," *Canadian Journal of Physics*, vol. 94, no. 5, pp. 490–496, 2016.

[37] M. Sheikholeslami and M. Sadoughi, "Mesoscopic method for MHD nanofluid flow inside a porous cavity considering various shapes of nanoparticles," *International Journal of Heat and Mass Transfer*, vol. 113, pp. 106–114, 2017.

[38] T. Hayat, S. Nadeem, and A. U. Khan, "Rotating flow of Ag-CuO/H2O hybrid nanofluid with radiation and partial slip boundary effects," *The European Physical Journal E*, vol. 41, no. 6, pp. 1–9, 2018.

[39] K. Loganathan, N. Alessa, and S. Kayikci, "Heat transfer analysis of 3-D viscoelastic nanofluid flow over a convectively heated porous Riga plate with Cattaneo-Christov double flux," *Frontiers of Physics*, vol. 9, article 641645, 2021.

[40] H. A. Nabwey and A. Mahdy, "Transient flow of micropolar dusty hybrid nanofluid loaded with Fe3O4-ag nanoparticles through a porous stretching sheet," *Results in Physics*, vol. 21, p. 103777, 2021.

[41] H. U. Rasheed, S. Islam, Z. Khan et al., "Computational analysis of hydromagnetic boundary layer stagnation point flow of nano liquid by a stretched heated surface with convective

conditions and radiation effect," *Advances in Mechanical Engineering*, vol. 13, no. 10, 2021.

[42] K. Loganathan, G. Muhiuddin, A. M. Alanazi, F. S. Alshammari, B. M. Alqurashi, and S. Rajan, "Entropy optimization of third-grade Nanofluid slip flow embedded in a porous sheet with zero mass flux and a non-Fourier heat flux model," *Frontiers of Physics*, vol. 8, p. 250, 2020.

[43] Zeeshan, "Second law and entropy generation analysis of magnetized viscous fluid flow over a permeable expandable sheet with nonlinear thermal radiation: Brownian and thermophoresis effect," *Advances in Mechanical Engineering*, vol. 14, no. 1, 2022.

[44] I. C. Liu and H. I. Andersson, "Heat transfer over a bidirectional stretching sheet with variable thermal conditions," *International Journal of Heat and Mass Transfer*, vol. 51, no. 15-16, pp. 4018–4024, 2008.

[45] J. L. G. Oliveira, C. Tecchio, K. V. Paiva, M. B. H. Mantelli, R. Gandolfi, and L. G. S. Ribeiro, "Passive aircraft cooling systems for variable thermal conditions," *Applied Thermal Engineering*, vol. 79, pp. 88–97, 2015.

[46] I. Waini, A. Ishak, and I. Pop, "Hybrid nanofluid flow and heat transfer past a vertical thin needle with prescribed surface heat flux," *International Journal of Numerical Methods for Heat & Fluid Flow*, vol. 29, no. 12, pp. 4875–4894, 2019.

[47] I. Waini, A. Ishak, and I. Pop, "Hybrid nanofluid flow on a shrinking cylinder with prescribed surface heat flux," *International Journal of Numerical Methods for Heat & Fluid Flow*, vol. 31, no. 6, pp. 1987–2004, 2021.

[48] I. Ahmad, M. Faisal, T. Javed, A. Mustafa, and M. Z. Kiyani, "Numerical investigation for mixed convective 3D radiative flow of chemically reactive Williamson nanofluid with power law heat/mass fluxes," *Ain Shams Engineering Journal*, vol. 13, no. 1, p. 101508, 2022.

[49] N. S. Khashi'ie, I. Waini, N. A. Zainal, K. Hamzah, and A. R. Mohd Kasim, "Hybrid nanofluid flow past a shrinking cylinder with prescribed surface heat flux," *Symmetry*, vol. 12, no. 9, p. 1493, 2020.

[50] M. Faisal, I. Ahmad, and T. Javed, "Dynamics of MHD tangent hyperbolic nanofluid with prescribed thermal conditions, random motion and thermo-migration of nanoparticles," *Journal of dispersion science and technology*, pp. 1–15, 2021.

[51] T. Javed, M. Faisal, and I. Ahmad, "Dynamisms of solar radiation and prescribed heat sources on bidirectional flow of magnetized Eyring-Powell nanofluid," *Case Studies in Thermal Engineering*, vol. 21, p. 100689, 2020.

[52] I. Ahmad, M. Faisal, and T. Javed, "Dynamics of copper–water nanofluid with the significance of prescribed thermal conditions," *Heat Transfer*, vol. 50, no. 5, pp. 4248–4263, 2021.

[53] S. Mosayebidorcheh, M. Vatani, M. Hatami, and D. Domiri Ganji, "Two-phase nanofluid thermal analysis over a stretching infinite solar plate using Keller box method (KBM)," *Iranian Journal of Chemistry and Chemical Engineering (IJCCE)*, vol. 37, no. 6, pp. 247–256, 2018.

[54] M. Faisal, I. Ahmad, and T. Javed, "Keller–box simulation for nonzero and zero mass fluxes of nanofluid flow impinging over a bi-directional stretching sheet: an unsteady mathematical model," *International Journal of Modern Physics C*, vol. 32, no. 4, p. 2150052, 2021.

[55] I. Ahmad, M. Faisal, and T. Javed, "Unsteady rotating flow of nanofluid with prescribed thermal aspects," *International Journal of Modern Physics C (IJMPC)*, vol. 32, no. 7, p. 2150093, 2021.

[56] A. Abbasi and W. Farooq, "A numerical simulation for transport of hybrid nanofluid," *Arabian Journal for Science and Engineering*, vol. 45, no. 11, pp. 9249–9265, 2020.

[57] M. Faisal, I. Ahmad, and T. Javed, "Numerical assessments of prescribed heat sources on unsteady 3D flow of Williamson nanoliquid through porous media," *Special Topics & Reviews in Porous Media: An International Journal*, vol. 12, no. 2, pp. 71–92, 2021.

[58] T. Sajid, W. Jamshed, F. Shahzad et al., "Study on heat transfer aspects of solar aircraft wings for the case of Reiner-Philippoff hybrid nanofluid past a parabolic trough: Keller box method," *Physica Scripta*, vol. 96, no. 9, article 095220, 2021.

[59] I. Ahmad, M. Faisal, and T. Javed, "Unsteady flow of Walters-B magneto-nanofluid over a bidirectional stretching surface in a porous medium with heat generation," *Special Topics & Reviews in Porous Media: An International Journal*, vol. 12, no. 3, pp. 49–70, 2021.